CHAPTER 2

SYNTHESIS AND CHARACTERIZATION OF PURE ZnO AND Nb-DOPED ZnO NANOPARTICLES

There are three parts in this chapter consisting of research overviews, experimental and results and discussion. In the first part, research overviews of synthesis of ZnO nanoparticles, flame spray synthesis of nanoparticles and flame spray pyrolysis based on pure ZnO and metal-doped ZnO. The second part, flame spray pyrolysis was employed to synthesize the nanopowders including the preparation of precursors and chemicals. In the third part, the characterization methods were employed to characterize the nanoparticles physical properties.

2.1 Research overviews

2.1.1 Synthesis of ZnO nanoparticles

ZnO nanoparticles have been mostly synthesized through wet-chemical methods such as precipitation [1], sol–gel [2] and hydrothermal [3] syntheses. Additionally, ZnO has been obtained in film form through techniques including pulsed laser deposition [4], sol–gel dip–coating [5], magnetron sputtering [6]. Various workers have been revealed on synthesis and characterization of different nanostructures of pure and doped zinc oxide. Spanhel and Anderson [7] have explained the synthesis of nano crystals of zinc oxide using distillation set–up starting with products of zinc acetate and ethanol. Using this technique they have obtained highly concentrated colloidal nanocrystals of ZnO of size varying from 3.5–5.5 nm

with ageing and shown that these crystals remain in a dispersed state for weeks. Hossain et al. [8] had further modified this technique successfully to obtain nanobelts of ZnO of length 700 μm using refluxing technique.

Nanocrystalline ZnO using $ZnCl_2 \cdot 2H_2O$ and $(NH_4)_2CO_3$ as raw materials by direct precipitation method was reported by Siqingaowa et al. [9]. The nanocrystalline ZnO was characterized using XRD, TEM and BET. Experimental results for nanocrystalline ZnO showed that the minimum size was about 8 nm, the maximum was about 15 nm and the mean grain size was 12 nm, the surface area was 80.56 m^2/g and the purity was 99.9% when the precursor was calcined at 300°C for 2h.

Nanocrystalline ZnO powders have been synthesized by means of a novel gel-network precipitation method using gelatin as a template at lower temperature condition were reported by Zhou et al. [10]. The products were characterized by using TG-DTA, XRD and TEM techniques. The products appeared to be regularly spherical or elliptical and their sizes range from 20 to 40 nm. The average particle size increased with increasing calcining temperature, and decreased with increasing gelatin concentration. Furthermore, the photoluminescence (PL) spectra of the ZnO nanopowders were also investigated. The relative luminescent intensities for the ultraviolet band and green emission band showed a dependence on preparation conditions.

Hydrothermal process was applied to synthesize zinc oxide nanocrystals by Chen et al. [3]. X-ray powder diffraction and scanning electron microscopy were used to analyze the crystal structure and surface morphology. XRD pattern analysis showed that the ZnO clusters are single hexagonal phase of wurtzite structure (space group P63mc) with no impurity of Zn and $Zn(OH)_2$. Also, SEM images revealed that the

size of a single ZnO crystal is between 200–500 nm in diameter and 2–5 μm in length.

Burunkaya et al. [11] synthesized aluminum doped zinc oxide (AZO) nanometric particles by hydrothermal method. Aluminum nitrate hydrate, aluminum sec-butoxide and zinc nitrate hydrate were used as the starting materials, and n-propanol and 2-butanol were used as solvents. Obtained products were subjected to powder-XRD, particle size measurement, TEM examination and AAS analysis. Single phase AZO particles were obtained at alcohol to zinc nitrate ratio of 35, acid to zinc nitrate ratio of 0.2, at 225ºC. Particle size was determined as 3.2 ± 0.4 nm from TEM examinations and as 1–2 nm from dynamic light scattering

Elilarassi and Chandrasekaran [12] synthesized nanocrystalline $Zn_{1-x}Ni_xO$ (x = 0.00, 0.02, 0.04, 0.06, 0.08) powders by a simple sol–gel autocombustion method. Structural and optical properties of the Ni-doped ZnO samples annealed at 800ºC are characterized using XRD, SEM, EDAX, UV-visible spectroscopy and photoluminescence (PL). XRD analysis reveals that the Ni-doped ZnO crystallizes in a hexagonal wurtzite structure and secondary phase (NiO) was observed with the sensitivity of XRD measurement with the increasing nickel concentration ($x \geq 0.04$). PL measurements of Ni-doped samples illustrated the strong UV emission band at ~3.02 eV, weak blue emission bands at 2.82 and 2.75 eV, and a strong green emission band at 2.26 eV. The observed red shift in the band gap from UV-visible analysis and near band edge UV emission with Ni doping may be considered to be related to the incorporation of Ni ions.

2.1.2 Flame spray synthesis of nanoparticles

Many new materials using nanoparticles require the non-agglomerated

spherical particles. For semiconductors, the particle size and shape must be well controlled to most efficiently exploit quantum confinement effects [13]. In gas sensors, small-sized particles decrease the response time and increase the gas sensitivity while a low degree of aggregation facilitates the production of thin films [14]. In photocatalysis, spherical titania nanoparticles show a higher activity for CO oxidation than polyhedric particles [15]. It is well known that the surface characteristics of ZnO, determined by the different fabrication processes, will influence the optical properties as well as the final degradation efficiency [16]. FSP is a very promising technique for synthesis of high purity nanosized materials with controlled size and crystallinity. The method has been applied to prepare metal oxide-supported particles and heterogeneous catalysts. The characteristics of flame-made particles are controlled by reactant mixing, precusor, additives and electric fields that could be reviewed below.

Mädler et al. [17] investigated systematically the FSP process using an external-mixing gas-assisted atomizer supported by six premixed flamelets at production rates of 9 g/h. They studied the effect of oxidant and precursor fuel composition on the size of silica primary particle (7–39 nm) using as precursor hexamethyldisiloxane (HMDSO) dissolved in ethanol, iso-octane or methanol using air or O_2 as dispersion gas. Furthermore, with similar reactors, hollow or solid Bi_2O_3 were made at production rates up to 46 g/h as well as CeO_2 at production rates up to 10 g/h.

Kammler et al. [18] observed that the average primary particle diameter decreased from 25 to17 nm when increasing the oxidant (air) flow rate from 68 to 154 l/min in a turbulent H_2-air flame aerosol reactor at a silica production rate of 300 g/h

using HMDSO vapor as precursor. The obtained primary particle sizes are similar to the ones made here by FSP when using O_2 as dispersion gas. This indicates a similar control of primary particle diameter with oxidant flow rate at a constant powder production rate for both vapor- and liquid-fed flame reactors. Apparently, at high production rates, the precursor droplets rapidly evaporate during FSP resulting in particles similar to those made by conventional vapor-fed flame reactors.

Kammler et al. [18] investigated silica production rates from 125 to 700 g/h in a vapor-fed turbulent H_2-air flame reactor. The average primary particle diameter increased from 12 to 37 nm when increasing the HMDSO concentration in the reactant stream at an air flow rate of 103 l/min. Here, particle sizes of the vapor-fed flame lay within the operation window of the FSP reactor, which is an additional indication of particle formation in the gas rather than droplet phase with the FSP process. The operation window of the versatile FSP process at high production rates is similar to the ones of the well-established vapor-fed flame aerosol reactors which are used in industry for large-scale production.

2.1.3 Flame spray pyrolysis based on pure ZnO and metal-doped ZnO

Since the early 1970s, synthesis of fumed ZnO has been carried out to study the behavior of ZnO as air pollutant. Marshall et al. [19] first reported FSP fumed ZnO by spraying a zinc acetate aqueous solution into a gas-air burner to be used for toxicologic studies. Teague and Raabe [20] made a mixture of submicron-sized ZnO particles and aggregated ZnO nanoparticles with a mass median aerodynamic diameter of 800 nm by heating zinc acetate mist in a furnace at 1150ºC. Carroz et al. [21] produced hexagonal zincite (ZnO) particles of 200 nm in volume median diameter from a zinc nitrate in ethanol or methanol solutions by FSP.

McCarthy et al. [22] investigated industrial ZnO particle synthesis by the French process, evaporation and oxidation of Zn metal, in a hot wall reactor by varying the temperature and gas flow rate in the furnace. The ZnO particles were chain aggregates of primary nanoparticles (less than 30 nm), submicronsized blocky particles and acicular particles. Recently, demands for high product performance have necessitated a precise control of ZnO particle properties for high value applications such as electrode of solar cells and photocatalysts. Close attention is given to the high chemical reactivity of ZnO by increasing reactive sites and the complex nature of the UV and visible fluorescence. Therefore, a lot of effort has been taken to precisely control particle properties of ZnO by various sophisticated manufacturing processes.

Matsoukas and Friedlander [23] prepared inhomogeneous ZnO of d_{EM} = 10 nm from spray-dried zinc nitrate aerosol in a premixed methane-air flame, where also large particles (over 20–30 nm) were observed. Jensen et al. [24] made ZnO by oxidation of zinc acetylacetonate $(Zn\text{-}acac)_2$ in a premixed methane-air flame and found that the d_{BET} increased from 25 to 40 nm by increasing the concentration of $(Zn\text{-}acac)_2$ and decreasing the initial oxygen/methane ratio. Other energy sources were used for powder synthesis, such as laser vaporization and condensation of zinc metal [25], giving 10–15 nm ZnO particles, and plasma pyrolysis of zinc carbonate hydrate [26], resulting in 20 nm ZnO particles regardless of the feed rate. ZnO nanoparticle synthesis with different primary particle sizes (d_{EM} = 5–12 nm) was carried out also by spray pyrolysis using filter expansion aerosol generator (FEAG) at different furnace temperatures [27]. The particle size was much smaller than that expected from the concentration of the precursor (zinc acetate) and the dispersed droplet size, suggesting that the particles were formed in the gas phase in contrast to

conventional spray pyrolysis in which the reaction occurs in the liquid phase [28]. Inductively coupled plasma [29] and furnace heating [30] were applied to make rod-like and acicular ZnO particles, respectively, although both product particles were rather large (d_{EM} > 50 nm). In addition, spray pyrolysis of zinc nitrate or acetate [31], hydrothermal gas discharging of zinc acetate [32] and fuel combustion of zinc nitrate [33] were investigated to make rather large (d_{EM} > 50 nm) ZnO particles.

Tani et al. [34] made ZnO nanoparticles by FSP of zinc acrylate-methanol-acetic acid solution. The effect of solution feed rate on SSA_{BET} and crystalline size was examined. The average primary particle diameter can be controlled from 10 to 20 nm by the solution feed rate. All powders were crystalline zincite. Increasing the solution feed rate increases the flame height, and therefore coalescence and/or surface growth was enhanced, resulting in larger primary particles. Compared with ZnO nanoparticles made by other processes, the FSP-made powder exhibits some of the smallest and most homogeneous primary particles. Furthermore, the FSP-made powder has comparable BET equivalent primary particle diameter with but higher crystallinity than sol-gel derived ZnO powders.

Tani et al. [35] synthesized ZnO powders by FSP. Zinc acetate dihydrate was used as Zn source. The precursors was dissolved in methanol and deionized water mixture with volume ratios of methanol/water = 100/0, 80/20, 60/40 and 40/40, resulting in 0.5 mol/L precusor solutions. The product powders were characterized by nitrogen adsorption, infrared adsorption (IR), XRD and TEM. The effects of solvent on powder characteristics were examined by changing method content (1–0.4) in the solvent. Polyhedral aggregates of nanoparticles were formed from the precursor solution with x=1–0.6 for ZnO synthesis, suggesting complete evaporation of the

metal species and particle formation in the gas phase. Decrease of the methanol content to x=0.4 lowered the spray flame temperature, suppressing complete evaporation, resulting in a mixture of nanoparticles and large (e.g.>100 nm) particles for ZnO synthesis.

Height et al. [36] synthesized of inorganic nanorods with closely controlled aspect ratio by FSP-a single step, continuous, and scalable process. Zinc oxide doped with In, Sn or Li up to 10 at% exhibited a single-phase wurtzite structure. In and Sn dopants, however, alter progressively the shape of the ZnO particles to a rodlike shape with increasing dopant concentration. Sn has a stronger nanorod-forming influence than in at low dopant levels. Lithium does not influence the shape of the ZnO. The XRD lattice aspect ratio for both the In- and Sn-doped ZnO crystals was increased by a factor of 5 as dopant content increased up to 10 at% and was confirmed by TEM. The SSA_{BET} for In- and Sn-doped ZnO increased with dopant concentration, with Sn giving a steeper increase, consistent with XRD indicating that for equivalent dopant concentration Sn gives a stronger nanorod-forming effect at lower loading than In.

Height et al. [37] synthesized of high surface area Ag-ZnO catalysts by FSP. Zinc naphthanate and silver nitrate were used as zinc and silver precursors, respectively. The Ag loading (1–5 at%) controlled the Ag cluster size from 5 to 25 nm but did not influence the ZnO crystal size. The SSA_{BET} was measured by five-point nitrogen adsorption and the equivalent average primary particle diameter (d_{BET}) was calculated using $d_{BET} = 6/(SSA_{BET} \times \rho_{ZnO})$ where ρ_{ZnO} is the powder density are showed in Table 2.1. Photodegradation of 10 ppm methylene blue (MB) solution was used to evaluate the performance of these FSP-made Ag-ZnO and was compared to wet-made Ag-ZnO and reference titania photocatalysts. The rate of photodegradation

was optimal for Ag loading around 3 at%. The best photocatalytic performance was exhibited by flame-made Ag-ZnO produced at the longest high-temperature residence times having high crystallinity.

Hui Li et al. [38] synthesised the Mg- and In-doped zinc oxide ($Mg_xZn_{1-x}O$, $In_yZn_{1-y}O$) nanoparticles by flame spray method. The XRD, SEM, and TEM analyses revealed that the morphologies of $Mg_xZn_{1-x}O$ or $In_yZn_{1-y}O$ nanoparticles were not very different, except for the change in the lattice constants. The UV-vis absorption spectra indicated that the band gap of $Mg_xZn_{1-x}O$ increased and that of $In_yZn_{1-y}O$ nanoparticles decreased. Moreover, the photoluminescence of the samples showed that the strong a near-band-edge (NBE) emission aroused by the exciton emission and weak visible emission by the defects produced in the process of preparation. The Burstein-Moss effects (BM) effects and exciton effects were used to explain the doping influence on the NBE emission and visible emission.

Table 2.1 Ag-ZnO catalysts prepared via FSP (3/8, 5/5, 8/3) and wet-phase synthesis together with measured SSA and reaction performance in photodegradation of MB.

Method	Sample	BET (m^2/g)
FSP (flame 3/8)	ZnO	119.4
	1% Ag-ZnO	115.6
	3% Ag-ZnO	101.6
	5% Ag-ZnO	87.6
FSP (flame 5/5)	ZnO	65.0
	1% Ag-ZnO	62.3
	3% Ag-ZnO	60.4
	5% Ag-ZnO	59.6
FSP (flame 8/3)	ZnO	35.5
	1% Ag-ZnO	36.0
	3% Ag-ZnO	38.3
	5% Ag-ZnO	33.4
Wet-made	ZnO	6.4
	1% Ag-ZnO	7.9
	3% Ag-ZnO	5.9
	5% Ag-ZnO	6.4

2.2 Experimental

2.2.1 Chemicals and equipments

- Zinc naphtenate (Aldrich, 8wt% Zn)
- Niobium (V) ethoxide (Aldrich, 99.95%)
- Toluene (Aldrich, 99%, Merck)
- Methanol (Labscan, analytical sciences)
- Acetonitrile (Fluka, 99.5%,)
- Ethanol (Labscan, Absolute for analysis)
- Hexane (Aldrich, 99%, Merck)
- Acetic acid (Riedel deHaen, 99%,)
- Xylene (Aldrich, 99%, Merck)
- Dichlomethene (Labscan, analytical sciences)
- Isopropanol (Labscan, analytical sciences)
- Acetone (Labscan, analytical sciences)
- Methane gas (Pangas, Germany)
- Oxygen gas (Pangas, Germany)
- Syringe pump (Inotech, Germany)
- Glass microfiber filters (Whatmann GF/A, 25.7 cm in diameter)
- Vacuum pump (Busch, Seco SV 1040C, Germany)

2.2.2 Solubility test

Prior to the precursor preparation, the zinc naphthenate and niobium (V) ethoxide were tested in the solubility test with several organic solvents as shown in Figures 2.1 and 2.2

Figure 2.1 The solubility tests of the precursors were performed using zinc napthenate as a Zn precursor dissolved in several organic solvents prior to the precursor preparation.

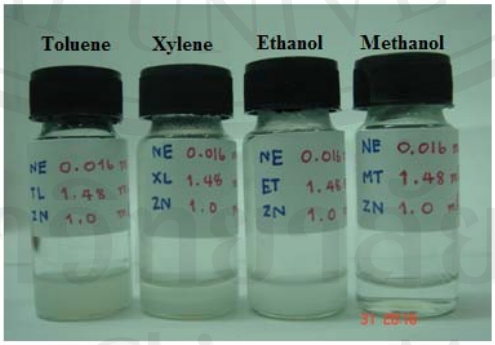

Figure 2.2 The solubility tests of the precursors were performed using niobium (V) ethoxide as a Nb precursor dissolved in several organic solvents prior to the precursor preparation.

This is because the solubility test and the homogeneous of the precursor mixtures were also affected the processing of FSP. Moreover, the most appropriate solvent is directly affected the particle formation in terms of the combustion enthalpy. This factor plays an important role in controlling the particle sizes by providing the combustion rate for the particles formation in flame. The solubility activity was shown in Figure 2.1 for a zinc naphthenate dissolved in various organic solvents, Figure 2.2 for a niobium (V) ethoxide dissolved well in methanol and Figure 2.3 for a zinc naphthenate and niobium (V) ethoxide dissolved well in toluene:methanol mixture with ratio of 70:30 vol% prior to the precursor preparation.

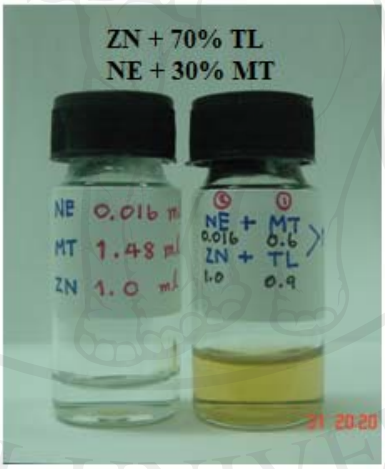

Figure 2.3 The solubility tests of the precursors were performed using zinc napthenate and niobium (V) ethoxide as Zn and Nb precursors dissolved well in toluene:methanol mixture with ratio of 70:30 vol% prior to the precursor preparation.

2.2.3 Precursor preparation for FSP

The volume of 100 mL with concentration of 0.5 mol/L of precursors were prepared for synthesizing the pure ZnO and 0.10, 0.25, 0.50, 0.75, 1.00, 2.00, 3.00 mol% Nb-doped ZnO the procedure below.

- Zinc Naphthenate was measured by the volumes that were calculated for synthesizing the pure ZnO, 0.10 mol% Nb-doped ZnO, 0.25 mol% Nb-doped ZnO, 0.50 mol% Nb-doped ZnO, 0.75 mol% Nb-doped ZnO, 1.00 mol% Nb-doped ZnO, 2.00 mol%, Nb-doped ZnO and 3.00 mol% Nb-doped ZnO as follows: 42.48, 42.43, 42.37, 42.26, 42.05, 41.63 and 41.20 mL, respectively.
- Niobium (V) ethoxide was measured by the volumes that were calculated as the dopants in 0.10-3.00 mol% Nb-doped ZnO as follows: 0.013, 0.031, 0.065, 0.094, 0.125, 0.251 and 0.376 mL, respectively.
- Zinc naphthenate and niobium (V) ethoxide were dissolved in toluene/methanol (70/30 vol%) to obtain the volume of 100 mL. These precursors had the concentration of 0.5 mol/L.

Table 2.2 Precursor preparation for FSP.

Flame-made (5/5) 0–3 mol% Nb-doped ZnO nanoparticle								
Doping				Combustion Entralpy				
precusor	CAS No.	density (g/ml)	molecular weight (g/mol)	precusor	CAS No.	density (g/ml)	Δc H°	
Zinc naphthenate (< 8 wt% Zn)	12001-85-3	0.962	-	Zinc	12001-85-3	0.962	25.4	KJ/ml
Niobium (V) ethoxide	3236-82-6	1.268	318.21	naphthenate				
Elements		molecular weight (g/mol)		(< 8 wt% Zn)				
Zn		65.38		Niobium (V)	3236-82-6	1.268		
O		16		ethoxide				
Nb		92.9064		Toluene (TL)	108-88-3	0.865	36.8	KJ/ml
ZnO		81.38		Methanol (MT)	67-56-1	0.791	17.9	KJ/ml

Precusors	mol% Nb	Niobium (V) ethoxide (ml)	mol% ZnO	Zinc naphthenate (ml)	Methanol (ml) 30%	Toluene (ml) 70%	Yield (g)
undoped ZnO	-	-	1.0000	42.48	17.26	40.27	4.069
ZnO : Nb 0.1mol%	0.0010	0.013	0.9990	42.43	17.27	40.29	4.070
ZnO : Nb 0.25 mol%	0.0025	0.031	0.9975	42.37	17.28	40.32	4.070
ZnO : Nb 0.5 mol%	0.0050	0.063	0.9950	42.26	17.30	40.37	4.072
ZnO : Nb 0.75 mol%	0.0075	0.094	0.9925	42.16	17.32	40.42	4.073
ZnO : Nb 1 mol%	0.0100	0.125	0.9900	42.05	17.35	40.48	4.075
ZnO : Nb 2 mol%	0.0200	0.251	0.9800	41.63	17.44	40.69	4.081
ZnO : Nb 3 mol%	0.0300	0.376	0.9700	41.20	17.53	40.89	4.086

2.2.4 Procedures for synthesizing nanoparticles by FSP

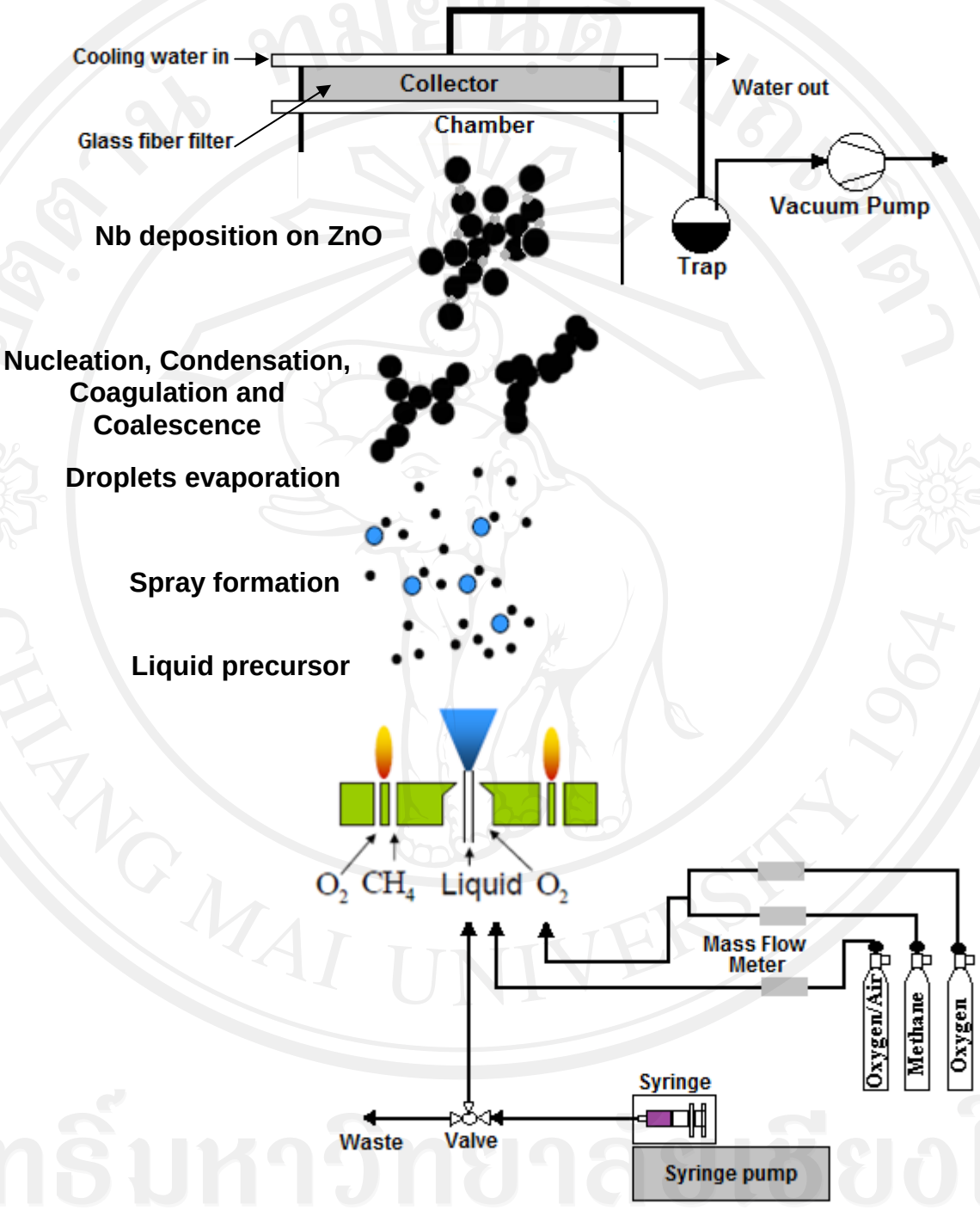

Figure 2.4 The experimental setup for flame-made pure ZnO and Nb-doped ZnO nanoparticles.

Pre-run setup includes running of the air-handling unit on operation mode, pilot flame, the extraction and the dispersing gas. A 1 L syringe is filled up with appropriate solution containing fuel and precursor (50 mL), placed in the holder with a driver. The precursor mix is fed into the nozzle and the solution is sprayed using a dispersing gas, typically air or O_2. Both the precursor feed rate and dispersing gas flow rate can be adjusted to achieve a change in droplet size, which will in turn affect the particle size of the end product. With the high enthalpy organic solution used in our experiment, a small pilot flame is used as a heat source to ignite and sustain spray combustion. The production of the powder is monitored by using a particle counter in the extraction line, the temperatures pre and post-collection and the pressure in the precursor line as well as the pressure drop across the nozzle. The compressed air pulsations to the collection bags and extraction may be adjusted during the run to optimise powder collection. Once the run is completed, the precursor line and the nozzle are cleaned by spraying with ethanol.

The FSP gas-assist nozzle had a radial symmetric configuration with a stainless-steel capillary tube (inner diameter, ID of 0.60 mm; outer diameter, OD of 0.91 mm) at the central axis serving as the liquid feed nozzle. Immediately surrounding the capillary tube was a narrow annular gap, of adjustable cross-sectional area, that issues 5 L/min of oxygen for spray atomization of the liquid feed. The pressure drop across the nozzle was maintained at 1.5 bar during FSP operation. A narrow concentric orifice ring was supplied with a mixture of CH_4 (1.19 L/min) and O_2 (2.46 L/min) to serve as a premixed flamelet for ignition and support of the spray flame. A sheath gas flow of 3.92 L/min of oxygen was issued though an annular sintered metal frit to stabilize and contain the spray flame. The precursor liquid feed rate was 5 mL/min using a rate-controlled syringe pump and all gas flows were

metered using mass flow controllers (Alborg). A water-cooled, stainless-steel filter housing supported a glassfiber filter (Whatman GF/A; 25.7 cm diameter) for collection of the flame-produced powder sample with the aid of vacuum pump (Busch, Seco SV 1040C).

Figure 2.4 shows the experimental setup for the flame-made pure ZnO and Nb-doped ZnO nanoparticles containing 0.10–3.00 mol%Nb. Zinc naphthenate (Aldrich, 8 wt%Zn) and niobium (V) ethoxide (Aldrich, 99.999%) were used as precursors. The precursors were dissolved in toluene/methanol (70/30 vol%) to obtain a 0.5 mol/l precursor solution. In a typical run, the precursor was fed into a FSP reactor by a syringe pump with a rate of 5 ml/min while 5 l/min O_2 is being dispersed (5/5 flame). The gas flow rates of methane and O_2 supporting flamelets were 1.19, and 2.46 l/min, respectively. The pressure drop at the capillary tip was kept constant at 1.5 bars by adjusting the orifice gap area at the nozzle. After evaporation and combustion of precursor droplets, particles are formed by nucleation, condensation, coagulation, coalescence and Nb deposited on ZnO support. Finally, the nanopowders were collected on glass microfiber filters (Whatmann GF/D, 25.7 cm in diameter) with the aid of a vacuum pump.

2.2.5 Particle characterization method

The crystalline phase, morphology and size of the pure ZnO and Nb-doped ZnO nanoparticles were characterized by XRD, SEM and TEM. The SSA_{BET} of the nanoparticles was measured by nitrogen adsorption. The optical properties of ZnO samples were evaluated in term of UV-vis absorption spectra.

2.3 Results and discussion

2.3.1 Nanoparticles synthesis

2.3.1.1 Flame-made pure ZnO and Nb-doped ZnO nanoparticles

During the synthesis of nanoparticles, all samples showed the same height of flame was observed to be approximately 10–11 cm, and was increased slightly by increasing the combustion enthalpy. The combustion enthalpies are directly dependent on the particular solvent, starting materials and dopants. All samples showed a yellowish-orange flame. These results could be confirmed that Nb was used as a dopant did not affect the flame properties in FSP experiment as seen in Figure 2.5

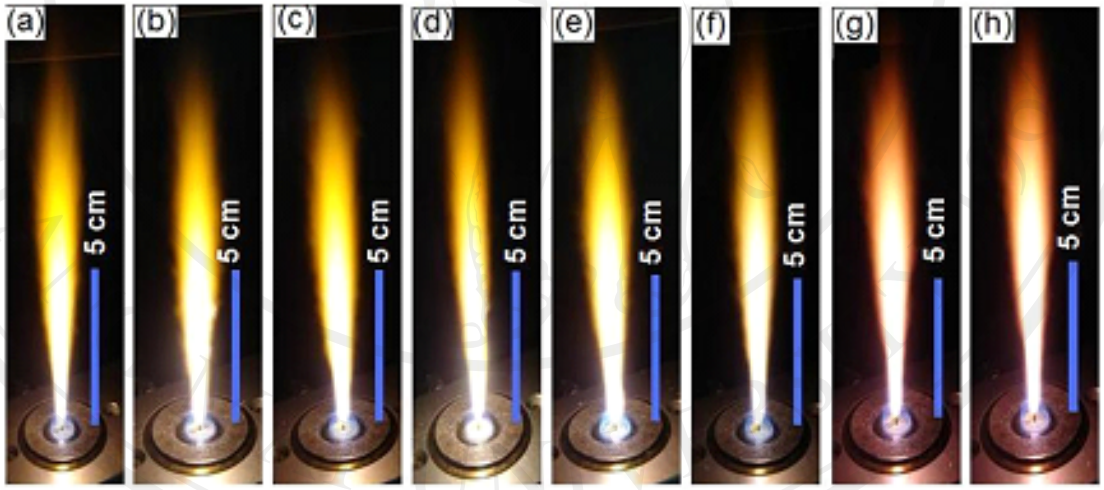

Figure 2.5 Spray flame (0.5 M zinc naphthenate and niobium (V) ethoxide in toluene/methanol: 70/30 vol%) of (a) pure ZnO, (b–h) 0.10–3.00 mol% Nb-doped ZnO nanoparticles producing 5 mL/min of liquid precursor feed rate and dispersed by O_2 (5 L/min) at 1.5 bar pressure drop across the nozzle tip. The flame heights were observed ranging from 10–11 cm.

2.3.1.2 Powder appearance

After flame synthesis, Figure 2.6 showed the appearance of pure ZnO and 0.10–3.00 mol% Nb-doped ZnO nanoparticles synthesized by FSP. It was found that all samples had the white color that had no difference among them. From this result, it can be concluded that both ZnO and Nb have white color and Nb does not effect to ZnO appearance.

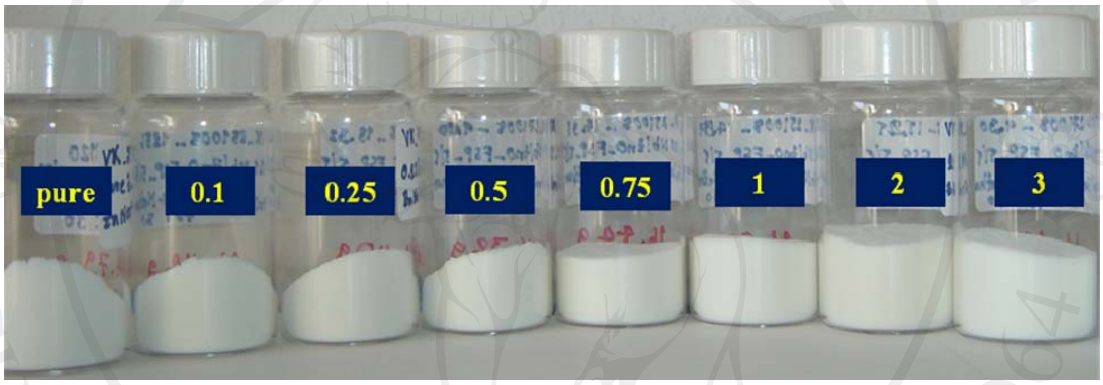

Figure 2.6 The flame-made (5/5) pure ZnO and 0.10-3.00 mol% Nb-doped ZnO nanoparticles ordered from the left to right with increasing Nb concentrations.

2.3.2 Characterization of flame-made nanoparticles

2.3.2.1 X-ray diffraction analysis

The phase and crystallinity of the flame-made nanopowders were analyzed by X-ray diffraction spectroscopy using CuKα radiation at 2θ = 20–80° with a step size of 0.06° and a scanning speed of 0.72°/min. Figure 2.7 shows the XRD patterns of the flame-made (5/5) pure ZnO and Nb-doped ZnO nanoparticles containing 0.10, 0.25, 0.50, 0.75, 1.00, 2.00 and 3.00 mol% Nb. It was found that all samples were highly crystalline, and all peaks can be confirmed to be the hexagonal structure of ZnO,

which match well with the JCPDS file No. 89-0510 [39]. Amorphous phase of ZnO and Nb peaks were not found in these patterns. It can be assumed that concentrations of Nb were too low and the sizes of Nb particles were too small, which affected the Nb peaks appearance. The intensity and sharpness of all diffraction patterns were not changed, indicating that the ZnO crystallinity did not change before or after doping with Nb.

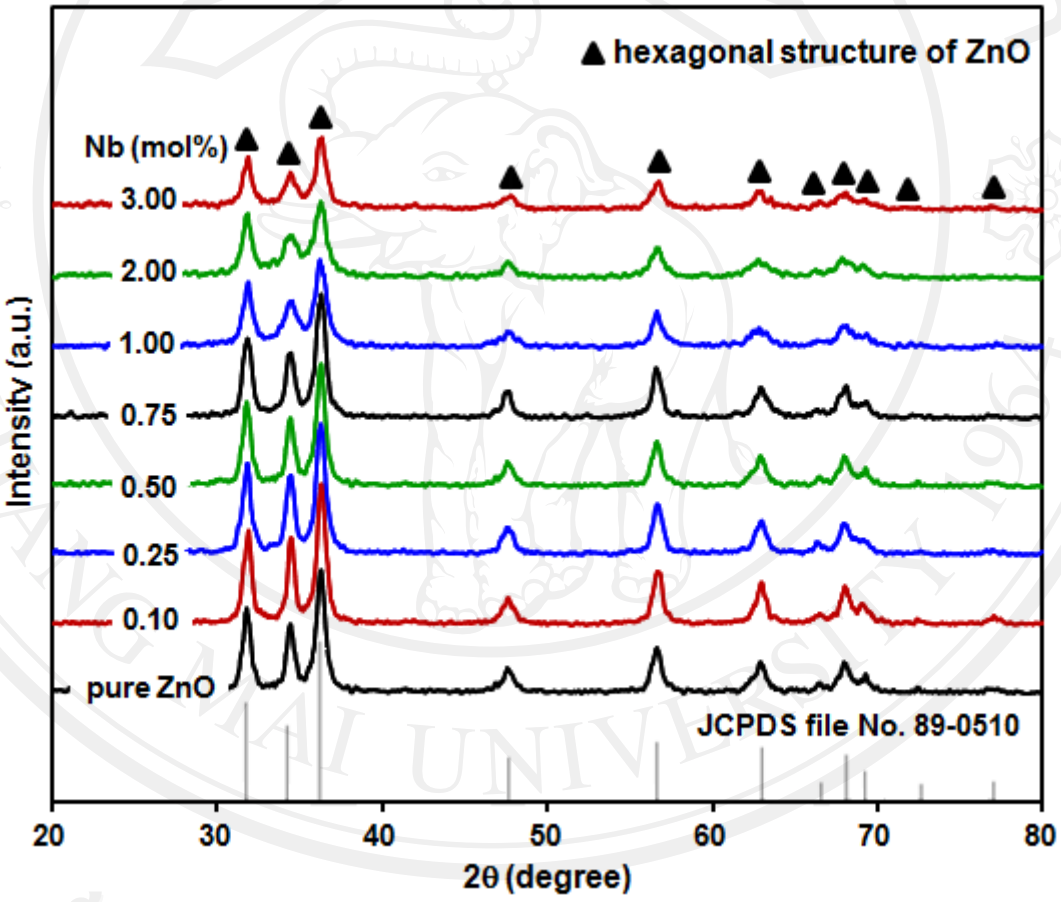

Figure 2.7 XRD patterns of the flame-made (5/5) pure ZnO and Nb-doped ZnO nanoparticles with different Nb concentrations.

2.3.2.2 BET analysis

The specific surface area (SSA_{BET}) of ZnO samples were measured by nitrogen absorption at 150ºC, using Brunauer-Emmett- Teller (BET) analysis (Micromeritics Tristar 3000). The average BET equivalent particle diameter (d_{BET}) were calculated using the average of the density of ZnO and Nb-doped ZnO taken into account for their weight content of different doping as shown in Figure 2.8, SSA_{BET} increased while the d_{BET} decreased with increasing Nb concentration from 0.10 to 3.00 mol%. When Nb particles were formed and deposited on the ZnO support processes in the flame, the Nb created a new nucleation center, which in turn changed the nucleation type from homogeneous to heterogeneous, and deteriorated the deposition forming leading to the agglomeration of the tiny Nb particles at high doping level. Accurate particles size and morphology of ZnO and Nb dispersion were confirmed by SEM and TEM images. The BET-particle diameter (d_{BET}) can be calculated using the formula as follows:

$$d_{BET} = \frac{6}{(\rho_{ZnO} \times SSA_{BET} \times wt\%ZnO) + (\rho_{Nb} \times SSA_{BET} \times wt\%Nb)} \qquad (2.1)$$

From equation 2.1 [37, 40], d_{BET} is the particle diameter, ρ_{ZnO} and ρ_{Nb} are the weight density of the ZnO (5.606 g/cm^3 [34]) and Nb (8.4 g/cm^3 [41]), respectively. Figure 2.8 shows the comparison of SSA_{BET} and d_{BET} of the pure ZnO and Nb-doped ZnO nanoparticles with different amount of Nb.

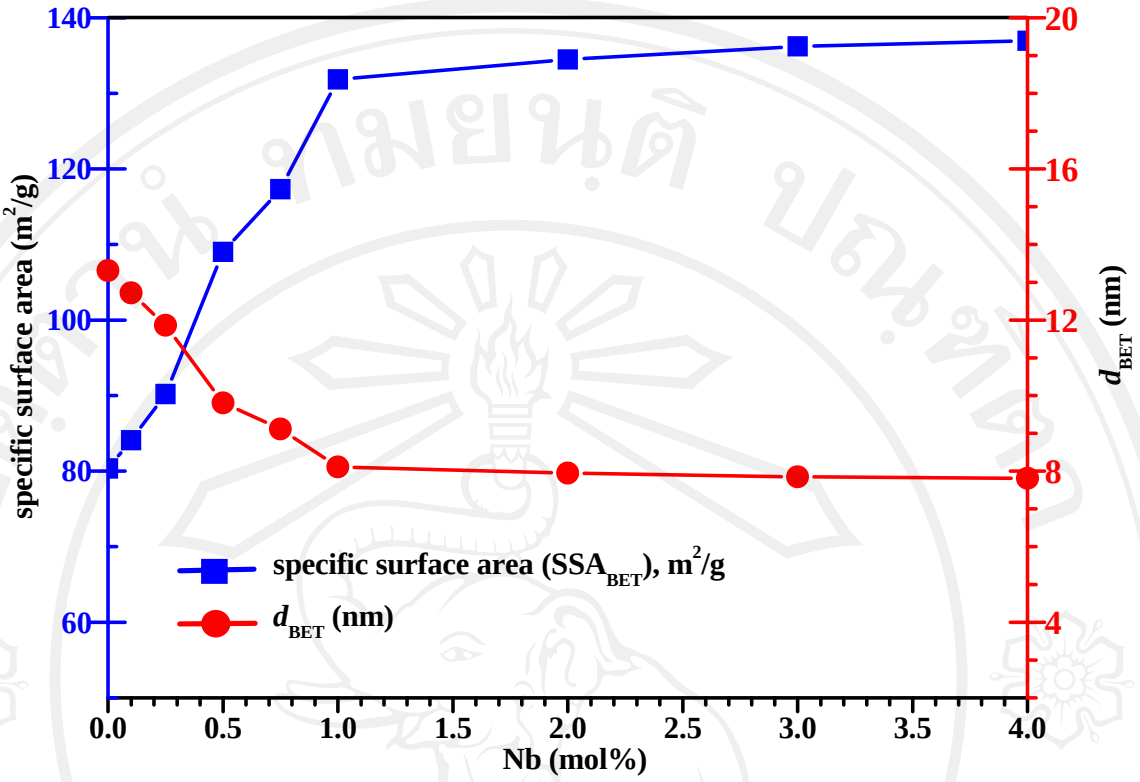

Figure 2.8 The specific surface area (SSA_{BET}) and BET-particle diameter (d_{BET}) of the flame-made (5/5) pure ZnO and Nb-doped ZnO nanoparticles with different Nb concentrations.

2.3.2.3 Transmission electron microscopy (TEM) and Energy dispersive x-ray spectroscopy (EDS)

TEM bright-field image of FSP-made pure ZnO and Nb-doped ZnO nanoparticles with 1.00 and 3.00 mol% metal loadings are shown in Figure 2.9. The images showed spherical nanoparticles along with a few nanorods. Spherical metal nanoparticles/ clusters dispersed on the surface of ZnO were clearly observed as the darker spots. Average diameters of Nb particles/clusters deposited on ZnO were determined to be approximately 1.5 nm for 1.00% Nb-doped ZnO nanoparticles. The crystallite sizes of ZnO spherical particles were found to be ranging from 5–20 nm.

ZnO nanorods were found to be ranging from 5–20 nm in width and 20–40 nm in length. The ZnO particle sizes and morphology were spherical, hexagonal and rod-like. From the TEM studies, the average size of the hexagonal type of ZnO nanoparticles was found to be 5–20 nm.

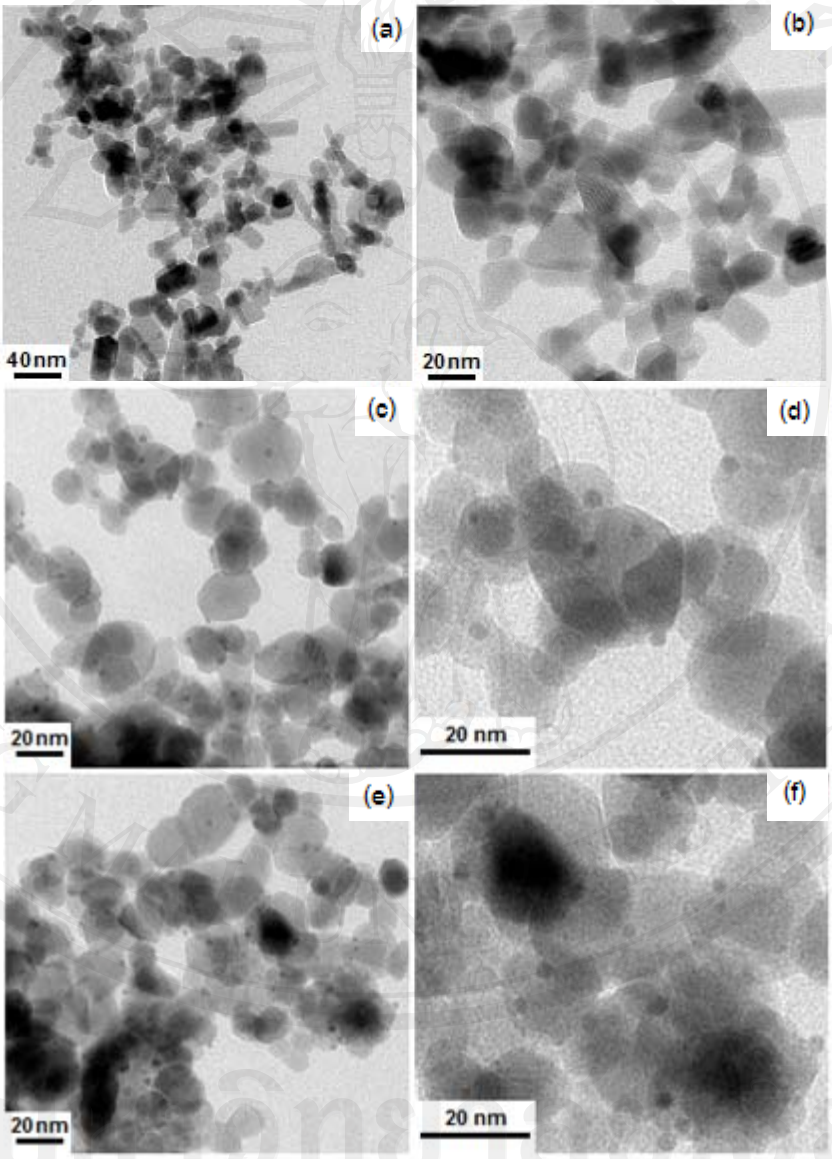

Figure 2.9 TEM bright-field image of (a, b) pure ZnO, (c, d) 1.00 mol% Nb-doped ZnO nanoparticles and (e, f) 3.00 mol% Nb-doped ZnO nanoparticles.

Figure 2.10 illustrates a TEM bright-field image and EDS analysis of 1.00 mol% Nb-doped ZnO nanoparticles. Figure 2.11–2.15 showed the EDS spectra of chemical elements of pure ZnO and 0.25, 0.50 1.00 and 3.00 mol% of Nb-doped ZnO nanoparticles. The signal of EDS spectrum corresponded to Nb, Zn and O elements. From these results, the Cu signal arose from the background support of copper grid. The element composition data from EDS confirmed niobium was actually in Nb-doped ZnO. However, the amount of element composition was slightly different depending on the different selected area of EDS analysis.

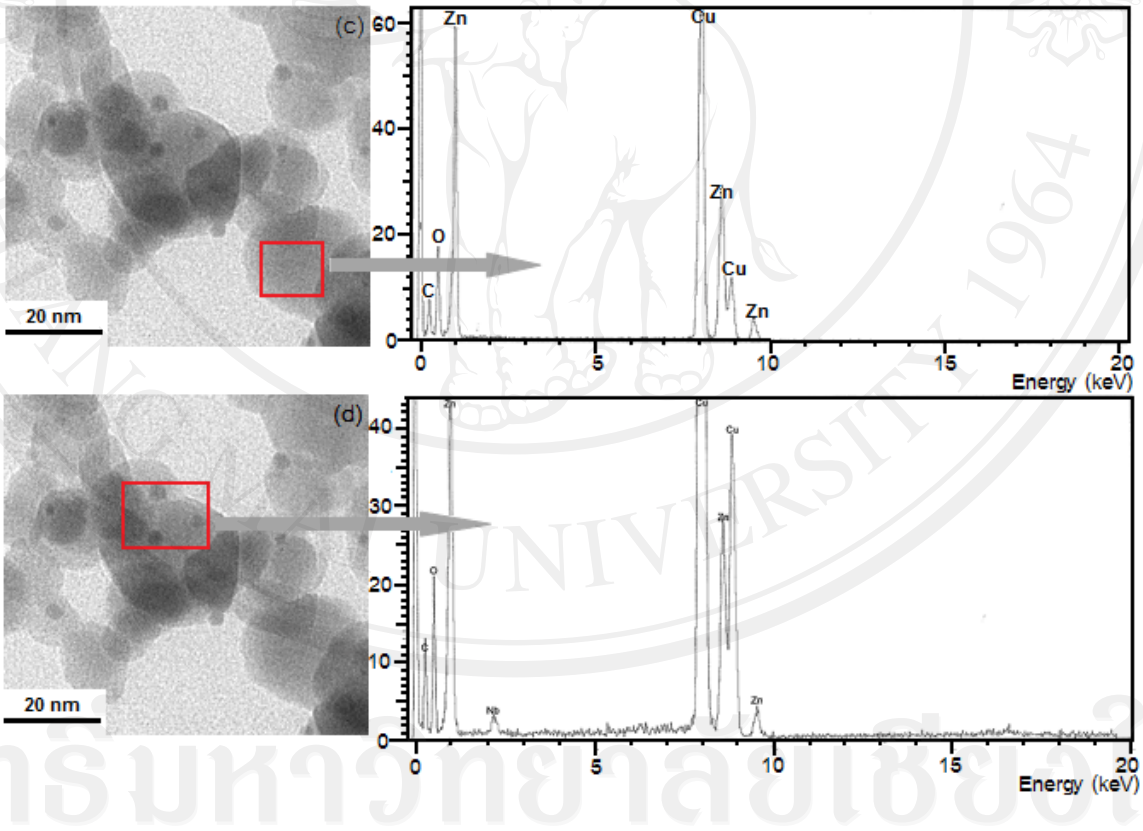

Figure 2.10 TEM bright-field image and EDS mode of 1.00 mol% Nb-doped ZnO.

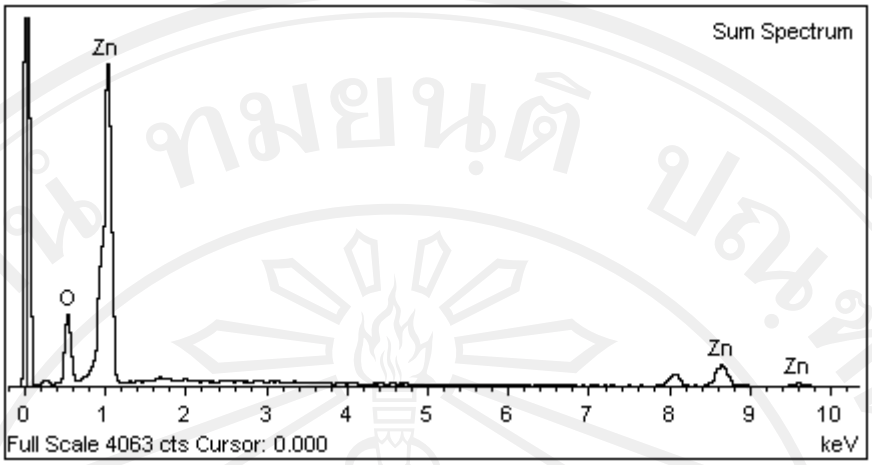

Figure 2.11 EDS spectrum (line scan mode) of pure ZnO nanoparticles.

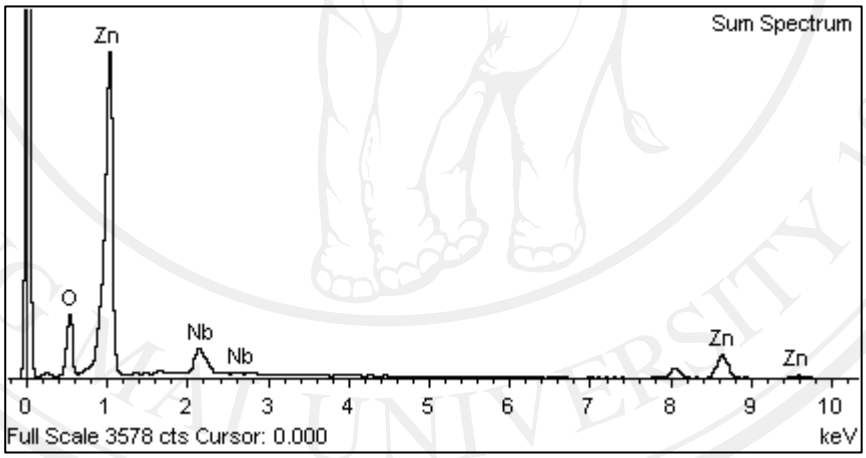

Figure 2.12 EDS spectrum (line scan mode) of 0.25 mol% Nb-doped ZnO nanoparticles.

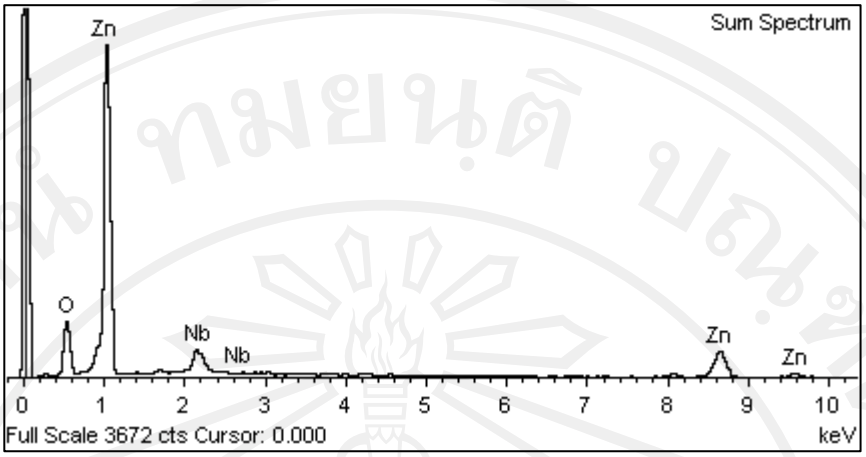

Figure 2.13 EDS spectrum (line scan mode) of 0.50 mol% Nb-doped ZnO nanoparticles.

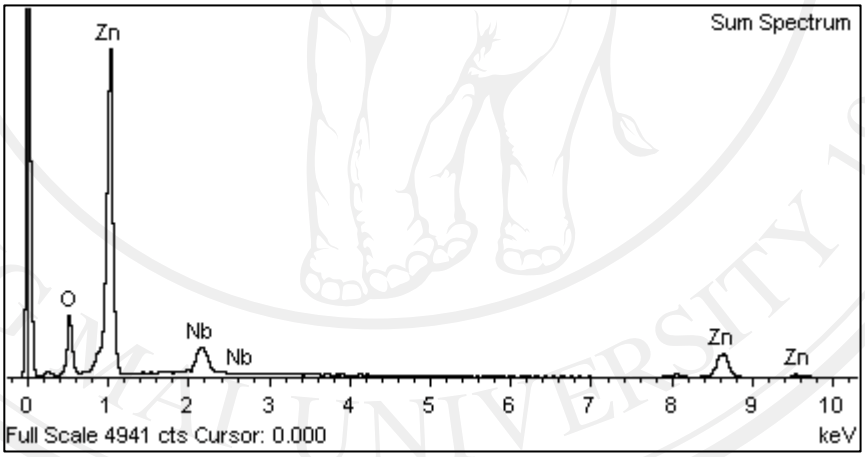

Figure 2.14 EDS spectrum (line scan mode) of 1.00 mol% Nb-doped ZnO nanoparticles.

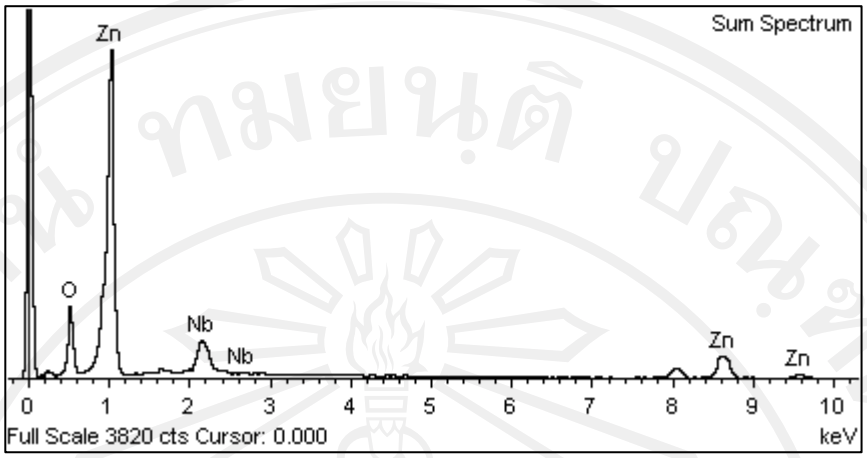

Figure 2.15 EDS spectrum (line scan mode) of 3.00 mol% Nb-doped ZnO nanoparticles.

2.3.2.4 Scanning Electron Microscopy (SEM) and Energy Dispersive X-ray Spectrometry (EDS): dot-mapping modes

Figures 2.16–2.20 show the scanning electron micrographs and EDS dot-mapping patterns of the ZnO and Nb-doped ZnO nanoparticles. The particles sizes of ZnO nanoparticles were in the range of 5–20 nm. In contrast, the ZnO nanoparticles, the Nb dispersed on the ZnO supported, and the corresponding elements also appeared in terms of the EDS dot-mapping probably due to agglomeration of the whole particles. The elemental dot mapping were identified by running the count frame for 40 cycles corresponding to the red spots show O content, green spots show Zn content and blue spots show Nb content. The EDS dot-mapping of all elements suggested a uniform distribution of Nb dispersed on the ZnO supported particles.

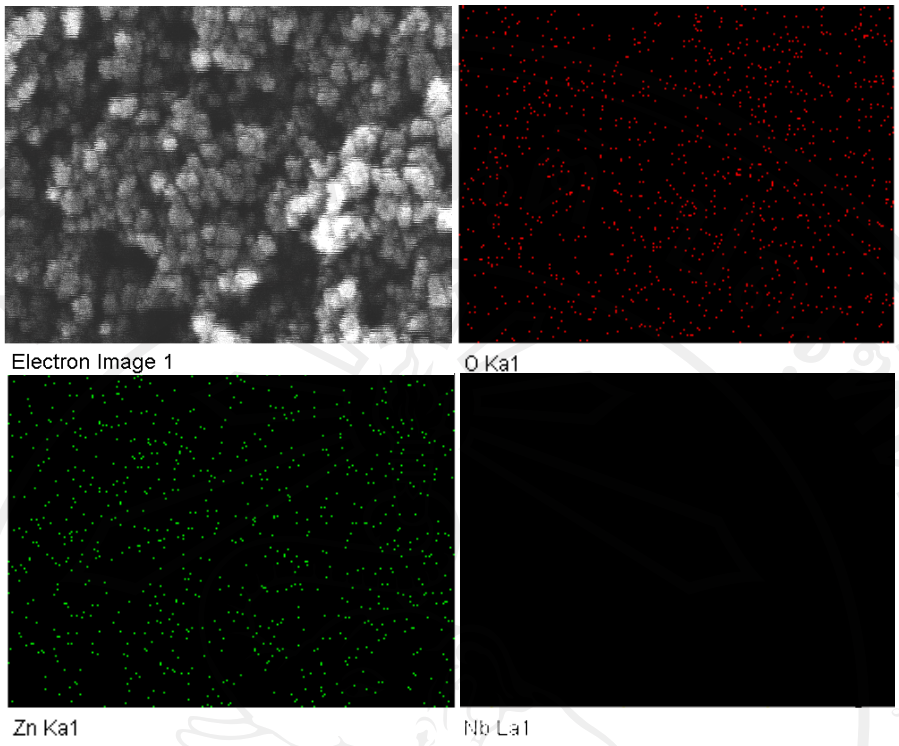

Figure 2.16 SEM image and EDS dot-mapping modes of the flame-made (5/5) pure ZnO nanoparticles.

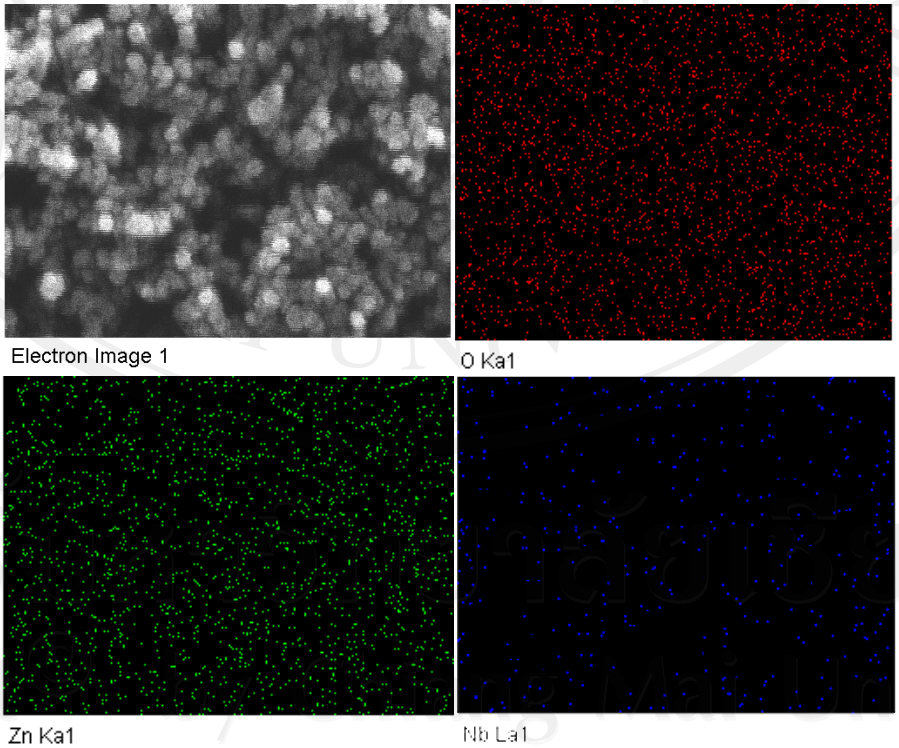

Figure 2.17 SEM image and EDS dot-mapping modes of the flame-made (5/5) 0.25 mol% Nb-doped ZnO.

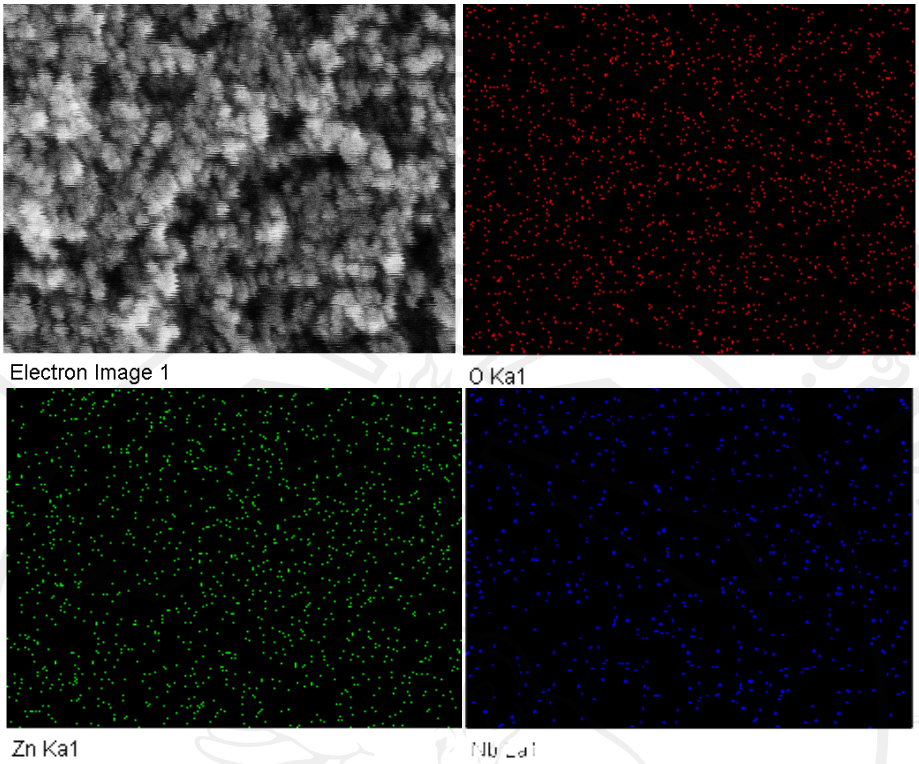

Figure 2.18 SEM image and EDS dot-mapping modes of the flame-made (5/5) 0.50 mol% Nb-doped ZnO.

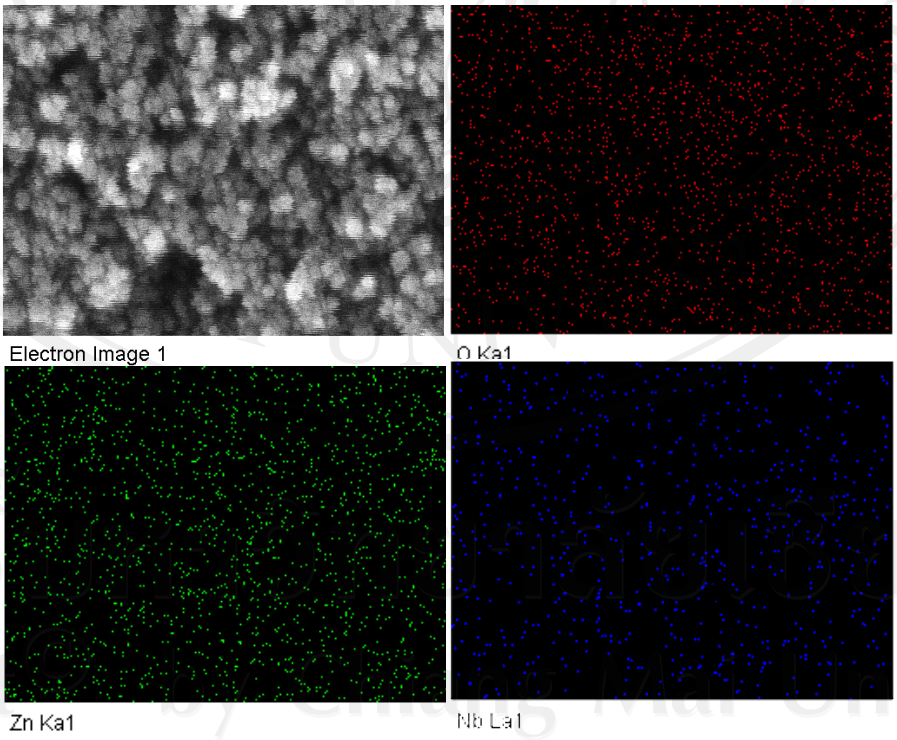

Figure 2.19 SEM image and EDS dot-mapping modes of the flame-made (5/5) 1.00 mol% Nb-doped ZnO.

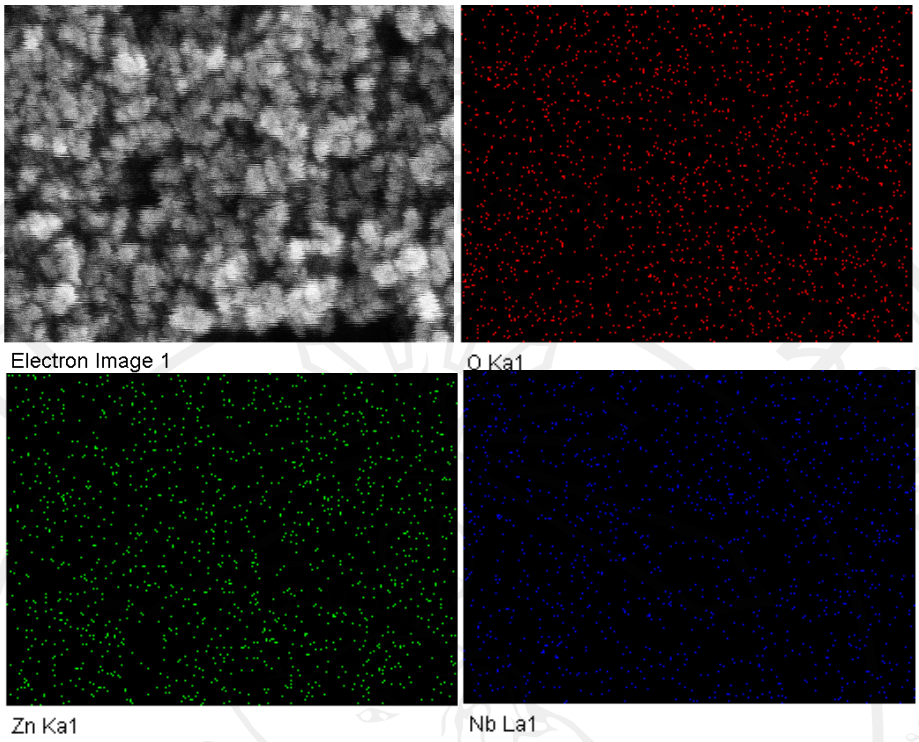

Figure 2.20 SEM image and EDS dot-mapping modes of the flame-made (5/5) 3.00 mol% Nb-doped ZnO.

2.3.2.5 UV-vis absorption spectroscopy

The optical properties of ZnO samples were evaporated by UV-vis absorption spectroscopy (Varian Cary 50 UV-vis spectrophotometer) at room temperature. Deionized water was used as a reference. Figure 2.21 shows the absorption spectra of pure ZnO and Nb-doped ZnO nanoparticles. It was found that the absorption spectra of ZnO doped with Nb at different ratio were quite similar to that of pure ZnO. The absorption edges of all samples were about 375 nm which were ascribed to the fundamental of pure ZnO, corresponding to the band-gab of about 3.2 eV. It can be concluded that Nb did not affect the ZnO structure. It was observed that the absorption intensity of ZnO slightly increased with increasing Nb content.

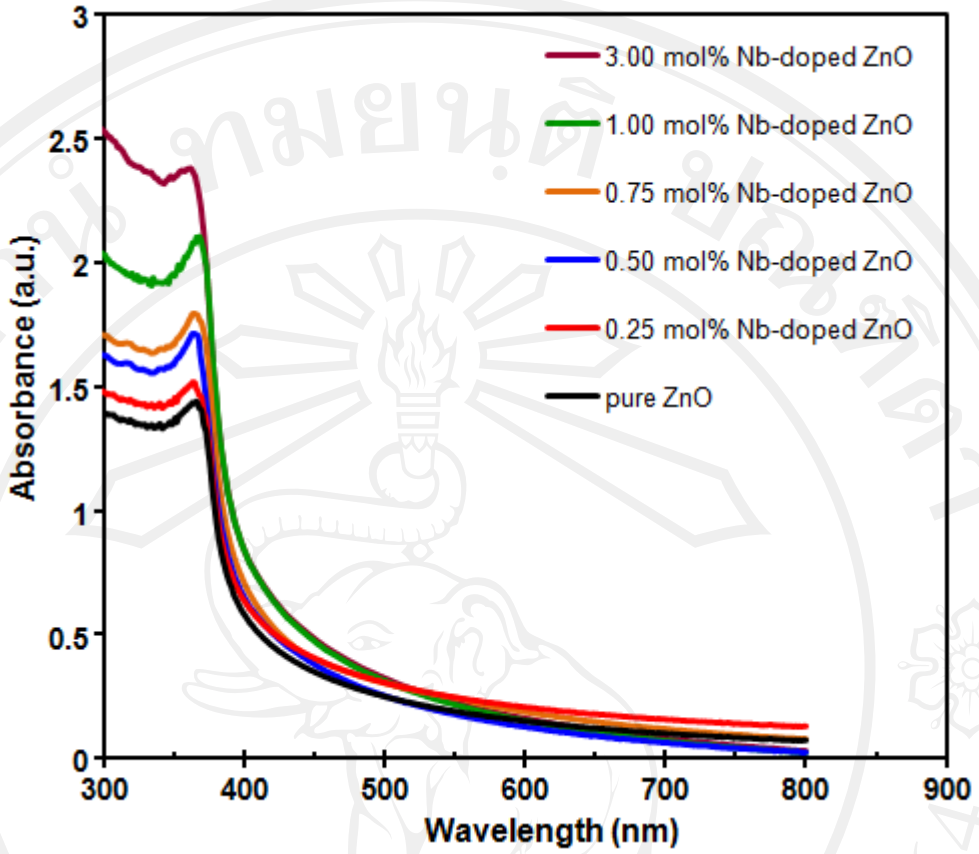

Figure 2.21 UV-vis absorption spectra of pure ZnO and Nb-doped ZnO nanoparticles with different Nb concentrations.

2.4 Conclusions

Flame spray pyrolysis (FSP) is a very promising technique for synthesis of high purity nano-sized materials with controlled size and crystallinity in one step. FSP was employed to synthesize pure ZnO and Nb-doped ZnO nanoparticles containing 0.10–3.00 mol% Nb. ZnO is one of the most versatile and most widely applied as catalytic metal oxide. Precursor solutions of zinc naphthenate and niobium (V) ethoxide in toluene/methanol (70/30 vol%) were sprayed and combusted under 5/5 (precursor/oxygen) flame condition, resulting in crystalline and nanostructured particles. The crystalline phase, morphology and size of the nanoparticles were characterized by XRD and TEM. The specific surface area of the nanoparticles was measured by nitrogen adsorption (BET analysis). The XRD patterns showed that the nanopowders were highly crystalline, and the peak can be confirmed to be the hexagonal structure of ZnO (JCPDS No. 89-0510). SSA_{BET} increased while the d_{BET} decreased with increasing Nb concentration. The ZnO nanoparticles were observed as particles having the clear spherical, hexagonal and rod-like morphologies. The crystallite sizes of ZnO spherical and hexagonal particles were in the range of 5–20 nm. ZnO nanorods were found to be ranging from 5–20 nm in width and 20–40 nm in length. The optical properties of ZnO samples were evaluated in term of UV-vis absorption spectra. The absorption spectra of ZnO doped with Nb at different ratio were quite similar to that of pure ZnO. The absorption edges of all samples were about 375 nm which were ascribed to the fundamental of pure ZnO, corresponding to the band-gab of about 3.2 eV. It can be concluded that Nb does not affect the ZnO structure. It was observed that the absorption intensity of ZnO slightly increased with increasing Nb content.

REFERENCES

1. Song R., Liu Y., He L., Synthesis and characterization of mercaptoacetic acid-modified ZnO nanoparticles, *Solid State Sci*, 2008, **10**, 1563–1567.
2. Ristic M., Music S., Ivanda M., Popovic S., Sol-gel synthesis and characterization of nanocrystalline ZnO powders, *J. Alloys Compd.*, 2005, **397**, 1–4.
3. Chen Y., Yu R., Shi Q., Qin J., Zheng F., Hydrothermal synthesis of hexagonal ZnO clusters, *Mater. Lett.,* 2007, **61**, 4438–4441.
4. Kim H., Horwitz J.S., Kim W.H., Makinen A.J., Kafafi Z.H., Chrisey D.B., Doped ZnO thin films as anode materials for organic light emitting diyotes, *Thin Solid Films,* 2002, **420**–**421**, 539–543.
5. Vale G.G., Hammer P., Pulcinelli S.H., Santilli C.V., Transparent and conductive ZnO: Al thin films prepared by sol–gel dipcoating, *J. Eur. Ceram. Soc.*, 2004, **24**, 1009–1013.
6. Yim K., Lee C., Optical properties of Al-doped ZnO thin films deposited by two different sputtering methods, *Cryst. Res. Technol.*, 2006, **41**, 1198–1202.
7. Spanhel L., Anderson M A., Semiconductor clusters in the sol-gel process: Quantized aggregation, gelation, and crystal growth in concentrated ZnO colloids., *J. Am. Chem. Soc.*, 1991, **113**, 2826–2833.
8. Hossain M. K., Ghosh S. C., Boontongkong Y., Thanachayanont C., Dutta J., Growth of zinc oxide nanowires and nanobelts for gas sensing applications, *J. Meta. Nanocrys. Mat.,* 2005, **23**, 27–30.

9. Siqingaowa, Zhaorigetu, Hongxia Y., Garidi, Preparation and characterization of nanocrystalline ZnO by direct precipitation method, *Front. Chem. China*, 2006, **3**, 277–280.

10. Zhou J., Zhao F., Wang Y., Zhang Y., Yang L., Size-controlled synthesis of ZnO nanoparticles and their photoluminescence properties, *J. Lumin.*, 2007, **122–123**, 195–197.

11. Burunkaya E., Kiraz N., Kesmez Ö., Ċamurlu H.E., Asiltürk M., Arpac E., Preparation of aluminum-doped zinc oxide (AZO) nano particles by hydrothermal synthesis, *J. Sol-Gel Sci. Techn.*, 2010, **55**, 171–176.

12. Elilarassi R., Chandrasekaran G., Synthesis, structural and optical characterization of Ni-doped ZnO nanoparticles, *J. Mater. Sci-Mater. El.*, 2010. in press.

13. Karthikeyan J., Berndt C.C., Tikkanen J., Wang J.Y., King A.H., Herman H., Nanomaterial powders and deposits prepared by flame spray processing of liquid precursors, *Nanostruct. Mater*., 1997, **8**, 61–74.

14. Mädler L., Kammler H.K., Mueller R., Pratsinis S.E., Controlled synthesis of nanostructured particles by flame spray pyrolysis, *J. Aerosol Sci,* 2002, **33**, 369–389.

15. Vemury S., Pratsinis S.E., Dopants in flame synthesis of titania, *J. Am. Ceram. Soc*., 1995, **78**, 2984–2992.

16. Fotou G.P., Scott S.J., Pratsinis S.E., The role of ferrocene in flame synthesis of silica, *Combust. Flame*, 1995, **101,** 529–538.

17. Mädler L., Kammler H.K., Mueller R., Pratsinis S.E. Controlled synthesis of nanostructured particles by flame spray pyrolysis, *J. Aerosol Sci,* 2002, **33**, 369–389.

18. Kammler H.K., Mueller R., Senn O., Pratsinis S.E., Synthesis of silica-carbon particles in a turbulent H_2-air flame aerosol reactor, *AIChE J.*, 2001, **47**, 1533–1543.

19. Marshall B.S., Telford I., Wood R., Afield method for the determination of zinc oxide fume in air, *Analyst,* 1971, **96**, 569–578.

20. Teague S.V., Raabe O.G., Generation of fume aerosols of zinc oxide, *Am. Ind. Hyg. Assoc. J.,* 1980, **41**, 680–683.

21. Carroz J.W., Odencrantz F.K., Finnegan W.G., Drehmel D.C., Aerosol generation to simulate specific industrial fine particle effluents, *Am. Ind. Hyg. Assoc. J.,* l980, **41**, 77–84.

22. McCarthy J.F., Yurek G.J., Elliott J.F., Amdur M.O., Generation and characterization of submicron aerosols of zinc oxide, *Am. Ind. Hyg. Assoc. J.,* 1982. **43**, 880–886.

23. Matsoukas T. Friedlander S.K., Dynamics of Aerosol Agglomerate Formation, *J. Colloid Interf. Sci.,* 1991, **146**, 495–506.

24. Jensen J.R., Johannessen T., Wedel S., Livbjerg H., Preparation of $ZnO–Al_2O_3$ particles in a premixed flame, *J. Nanopart. Res.,* 2000, **2**, 363–373.

25. Shall El M.S., Graiver D., Pernisz U., Baraton M.I., Synthesis and characterization of nanoscale zinc oxide particles: Laser vaporization condensation technique, *Nanostruct. Mater.,* 1995, **6**, 297–300.

26. Lin Y.H., Tang Z.L., Zhang Z.T., Yuan F.L., Ling Y.B., Lee J.L., Huang S.L., Preparation of nanometer zinc oxide powders by plasma pyrolysis technology and their applications, *J. Am. Ceram. Soc*., 2000, **83**, 2869–2871.

27. Kang Y.C., Park S.B., Effect of preparation conditions on the formation of primary ZnO particles in filter expansion aerosol generator, *J. Mater. Sci. Lett*., 1997, **16**, 131–133.

28. Messing G.L., Zhang S.C., Jayanthi G.V., Ceramic powder synthesis by spray-pyrolysis, *J. Am. Ceram. Soc.,* 1993, **76**, 2707–2726.

29. Suzuki M., Kagawa M., Syono Y., Hirai T., Synthesis of ultrafine single-component oxide particles by the spray–ICP technique, *J. Mater. Sci. Lett*., 1992, **27**, 679–684.

30. Baklanov A., Gorbunov B., Safatov A., Generator of ZnO particles with modified surface, *J. Aerosol Sci.,* 1999, **30**, 823–824.

31. Gardner T.J., Sproson D.W., Messing G.L., Precursor chemistry effects on development of particulate morphology during evaporative decomposition of solutions, *Mat. Res. Soc. Symp. Proc.,* 1984, **32**, 227–232.

32. Li W.J., Shi E.W., Tian M.Y, Zhong W.Z., Yin Z.W., The synthesis of ZnO acicular particles by the hydrothermal discharging-gas method, *J. Mater. Res*., l999, 14, 1532–1537.

33. Sousa de V.C., Morelli M.R., Kiminami R.H.G., Combustion process in the synthesis of ZnO-Bi_2O_3, *Ceram. Int.,* 2000, **26**, 561–564.

34. Tani T., Mädler L., Pratsinis S.E, Homogeneous ZnO nanoparticles by flame spray pyrolysis, *J. Nanopart. Res.,* 2002, **4,** 337–343.

35. Tani T., Kato A., Mosisaka H., Effect on powder characteristics of Zinc Oxide and Magnesia prepared by flame spray pyrolysis, *J. Ceram. Soc. Jpn.*, 2005, **113**, 255–258.

36. Height M.J., Mädler L., Pratsinis S.E., Nanorods of ZnO made by flame spray pyrolysis, *Chem. Mater.,* 2006, **18**, 572–578.

37. Height M.J., Pratsinis S.E., Mekasuwandumrong O., Praserthdam P., Ag-ZnO catalysts for UV-photodegradation of methylene blue, *Appl. Catal., B*, 2006, **63,** 305–312.

38. Li H., Zhang Y., Pan X., Zhang H., Wang T., Xie E., Effects of In and Mg doping on properties of ZnO nanoparticles by flame spray synthesis, *J. Nanopart. Res.,* 2009, **11**, 917–921.

39. Sawada H., Wang R., Sleigth A.W., An electron density residual study of zinc oxide, *J. Solid State Chem.,* 1996, **122**, 148–150.

40. Teoh W.Y., Mädler L., Beydoun D., Pratsinis S.E., Amal R., Direct (one-step) synthesis of TiO_2 and Pt/TiO_2 nanoparticles for photocatalytic mineralisation of sucrose, *Chem. Eng. Sci.*, 2005, **60**, 5852–5861.

41. Siddiki M.K., Munoz-Rojas D., Oro J., Jing J. u, Qia Q., Galipeau D. W. and ura-cantu M., Synthesis and Characterization of Nb doped Titania for Dye Sensitized Solar Cells, *IEEE Photovoltaic Specialists Conference*, 2009, 685–689.